Original Article

Quantitative assessment of corneal biomechanical changes in vivo after photorefractive intrastromal corneal cross-linking using optical coherence elastography

Hongwei Yang[1#], Yaoying Shen[2#], Yong Chen[3], Yange Yan[4], Yingjie Li[5], Yongan Lu[5], Jingchao Liu[5], Xiaolong Yin[1], Guofu Huang[1,6], Yanzhi Zhao[1]

[1]Department of Ophthalmology, The Second Affiliated Hospital, Jiangxi Medical College, Nanchang University, Nanchang, China; [2]Department of Pathology, Jiangxi Cancer Hospital, Nanchang, China; [3]Department of Anesthesiology, The Second Affiliated Hospital, Jiangxi Medical College, Nanchang University, Nanchang, China; [4]Yujiang District People's Hospital, Yingtan, China; [5]Department of Ophthalmology, The First Hospital of Nanchang, The Third Affiliated Hospital, Jiangxi Medical College, Nanchang University, Nanchang, China; [6]Zhongshan Ophthalmic Center, Sun Yat-sen University, Guangzhou, China

Contributions: (I) Conception and design: Y Zhao, G Huang, H Yang; (II) Administrative support: G Huang, X Yin; (III) Provision of study materials or patients: Y Shen, Y Chen, Y Li; (IV) Collection and assembly of data: Y Yan, Y Lu, J Liu; (V) Data analysis and interpretation: H Yang, Y Shen; (VI) Manuscript writing: All authors; (VII) Final approval of manuscript: All authors.

[#]These authors contributed equally to this work as co-first authors.

Correspondence to: Guofu Huang, MD. Department of Ophthalmology, The Second Affiliated Hospital, Jiangxi Medical College, Nanchang University, 1 Minde Road, Nanchang 330000, China; Zhongshan Ophthalmic Center, Sun Yat-sen University, Xianlie South Road 54, Guangzhou 510060, China. Email: hgf2222@sina.com; Yanzhi Zhao, MD. Department of Ophthalmology, The Second Affiliated Hospital, Jiangxi Medical College, Nanchang University, 1 Minde Road, Nanchang 330000, China. Email: 372779512@qq.com.

Background: Photorefractive intrastromal corneal cross-linking (PiXL) treatment corrects myopia by enhancing localized central corneal biomechanics. However, the dose-effect relationship between the changes in corneal biomechanics and alterations in corneal curvature resulting from this treatment remain unclear. We therefore developed an acoustic radiation force optical coherence elastography (ARF-OCE) technique to investigate the dose-effect relationship in PiXL.

Methods: ARF-OCE measurements and corneal topography were performed 3 days before and 1 week after PiXL treatment. Depth-resolved Young's modulus images of the in vivo corneas were obtained based on the phase velocity of the Lamb wave. PiXL treatments with five ultraviolet-A (UVA) energy doses (5.4, 15, 25, 35, and 45 J/cm^2) were administered to rabbit corneas *in vivo* (n=15).

Results: The percentage change in Young's modulus (ΔE%) of the cornea increased from 0.26 to 1.71 as the UVA energy dose increased from group I (5.4 J/cm^2) to group V (45 J/cm^2). Meanwhile, the change in the mean keratometry (ΔK_m) of the cornea increased from 0.40 to 2.10 diopters (D) as the UVA energy dose increased from group I to group IV (35 J/cm^2). Furthermore, a statistically significant positive correlation was observed between ΔE% and ΔK_m in groups I to IV.

Conclusions: With increasing UVA energy dose, the corneal Young's modulus significantly increased. Given the observed correlation, ΔE% holds promise as a new quantitative biomechanical parameter for determining the dose-effect relationship in PiXL treatment. It should be emphasized that there may be an inflection point of ΔE%, at which corneal keratometry ceases to flatten and begins to increase. The ARF-OCE system has demonstrated its efficacy in quantitatively assessing changes in corneal biomechanics *in vivo* following PiXL treatment. This technique has great potential in facilitating the quantitative determination of the dose-effect relationship in PiXL treatment.

Keywords: Optical coherence elastography (OCE); photorefractive intrastromal corneal cross-linking (PiXL); corneal biomechanics; ultraviolet-A energy dose (UVA energy dose)

Submitted Mar 23, 2024. Accepted for publication Aug 19, 2024. Published online Sep 26, 2024.
doi: 10.21037/qims-24-590
View this article at: https://dx.doi.org/10.21037/qims-24-590

Introduction

Photorefractive intrastromal corneal cross-linking (PiXL) is a relatively novel application of corneal collagen cross-linking (CXL) that is designed to correct mild myopia without removal of the corneal stroma (1-4). Compared with traditional refractive surgery, PiXL can reduce the risk of iatrogenic keratectasia, which is one of the most concerning complications of corneal refractive surgery (5). Conventional CXL utilizes ultraviolet-A (UVA) energy and riboflavin to create additional covalent crosslink bonds within collagen fibrils in the corneal stroma, which enhances corneal biomechanics (6). This conventional procedure uses UVA irradiation at 3 mW/cm^2 for 30 minutes to deliver a UVA energy dose of 5.4 J/cm^2 to the entire corneal surface. This dose has been shown to halt the progression of keratoconus (7). PiXL was designed based on conventional CXL to enhance corneal biomechanics in a small central region of the cornea. This approach flattens the central corneal curvature with subsequent myopic correction (3). Moreover, in PiXL, a customized pattern of UVA irradiation (30 mW/cm^2 and a 4-mm spot size) is applied to deliver higher total UVA energy doses to the central corneal region than those used in conventional CXL (3).

Although PiXL can correct myopia without removal of the corneal stroma, PiXL has several limitations as compared to traditional refractive surgery, including a limited correction range and lower precision. These limitations arise from an inexact determination of the dose-effect relationship in PiXL. Applying PiXL with different UVA energy doses may induce varying degrees of change in corneal biomechanics (dose), which in turn can lead to an array of alterations in corneal curvature (effect) (8-11). The dose-effect relationship should be investigated based on analyses of corneal biomechanical models or the outcomes of PiXL treatments. However, only a few varieties of PiXL treatments have been performed thus far, limiting the opportunities for comparisons that could clarify the effect of different energy doses. Consequently, employing an appropriate technique for the quantitative *in vivo* assessment of corneal biomechanical changes before and after PiXL is essential for studying the dose-effect relationship.

Currently, there is no universally accepted gold-standard clinical technique for measuring corneal biomechanics. The two commercial devices available for assessing corneal biomechanics include the ocular response analyzer and corneal visualization Scheimpflug technology. Although both devices detect the overall corneal response to air-pulse pressure, neither provide a quantitative assessment of corneal biomechanics, such as Young's modulus (12). Moreover, there are conflicting reports on whether these devices can be used to evaluate corneal biomechanical changes after CXL (13-16). In engineering, stress-strain extensometry is the gold-standard method for measuring macroscopic mechanical properties (17). However, this method requires cutting the cornea into strips and is thus unsuitable for *in vivo* applications. Therefore, the development of vivo quantitative techniques that can measure changes in corneal biomechanics following PiXL treatment are urgently needed.

Various elastography methods have been developed for the *in vivo* evaluation of tissue biomechanical properties, including magnetic resonance elastography, ultrasound elastography, and optical coherence elastography (OCE) (18-21). Magnetic resonance and ultrasound elastography are clinically available methods, but their relatively low resolution limits their application in the cornea. In contrast, OCE, which is based on optical coherence tomography (OCT), has emerged as valuable quantitative technique for assessing the biomechanical properties of ocular tissue (22-25). OCE uses OCT to detect elastic waves within the tissue that are caused by external excitation. The elastic wave velocity is positively correlated with tissue stiffness and can be quantitatively related to the Young's modulus of the tissue (26). Young's modulus is a classic biomechanical parameter that represents the ability of a material to withstand elastic deformation (27,28). Due to the high spatial resolution, fast imaging speed, and real-time imaging ability of OCT, OCE is well suited for biomechanical evaluation of the cornea. However, thus far, few studies have employed OCE to assess changes in corneal biomechanics following PiXL in living rabbits, especially under various

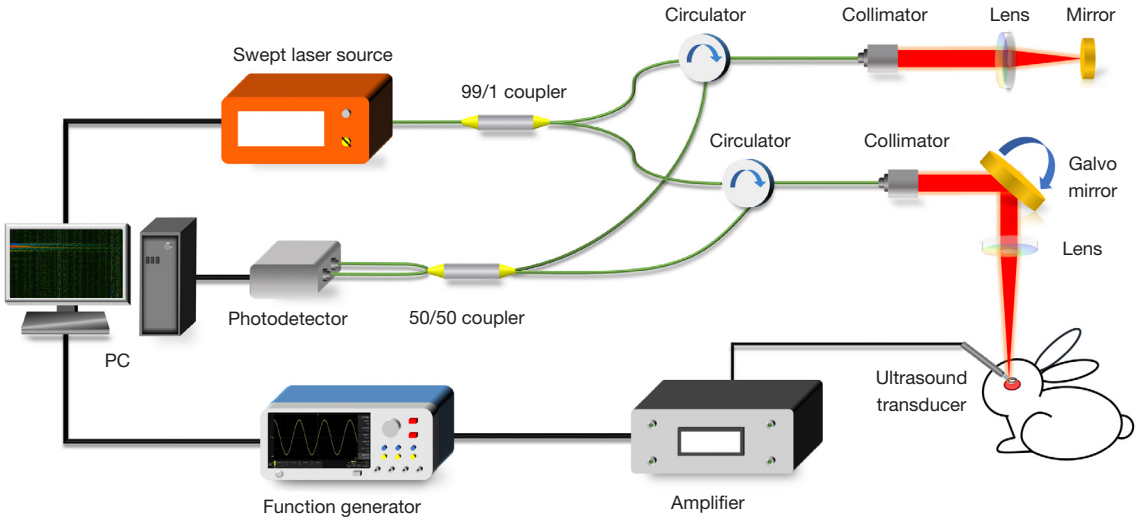

Figure 1 Schematic of the ARF-OCE system. PC, personal computer; ARF-OCE, acoustic radiation force optical coherence elastography.

UVA energy doses.

In our previous study, we designed an acoustic radiation force (ARF) OCE system and verified its feasibility and reliability in the cornea (29). In the present study, we developed an ARF-OCE system equipped with an ultrasmall ultrasound transducer. The new transducer excites the cornea via an ultrasonic coupling agent and is thus more suitable for *in vivo* applications as compared to previous approaches. Moreover, a Lamb wave model based on phase velocity was used to quantitatively assess rabbit corneal biomechanics under different PiXL energy doses. Furthermore, the dose-effect relationship in PiXL was investigated by analyzing the changes in the Young's modulus of the cornea and the corresponding alterations in the corneal curvature.

Methods

System setup

Figure 1 shows the laboratory-built ARF-OCE system, which is composed of a swept-source OCT unit and an ARF excitation unit. The swept-source laser (AXP50125-6; Axsun Technologies, Billerica, MA, USA) component of the OCT unit has a center wavelength of 1,310 nm, an A-line acquisition rate of 50 kHz, and an average power of 20 mW. The ultrasmall ultrasound transducer component in the ARF excitation unit has a center frequency of 930 kHz, an acoustic focal length of 0.8 mm, an outer diameter of 1.8 mm, and a focusing spot diameter of 1.6 mm. To drive the transducer to generate an ARF pulse, a burst signal with a center frequency of 930 kHz is produced using a function generator (AFG31102; Tektronix, Beaverton, OR, USA) and is amplified by a bandwidth amplifier (2100L-1328; Electronics & Innovation, Rochester, NY, USA). A more detailed description of the other elements in the two units can be found in our previous work (30). Based on our measurements, the OCT system has axial and lateral resolutions of 5.7 and 15 μm in air, respectively, with an imaging depth of 6 mm and a signal-to-noise ratio (SNR) of 105 dB.

Data acquisition and processing

The ARF-OCE system uses the M-B scanning mode to detect and map the propagation of elastic waves in the cornea. One M-scan consists of 500 A-lines captured in sequence at the same position. After the completion of one M-scan, the OCT beam is moved to the next lateral position by a galvanometer to repeat the same M-scan. As a result, one B-scan image includes 1,000 M-scans obtained at 1,000 positions. Furthermore, the ARF excitation is triggered between the 101st and 120th A-lines, resulting in 20 ultrasonic pulse excitations during each M-scan. The excitation and OCT scanning are synchronized with a λ trigger signal generated by the swept laser source.

The cornea is an anisotropic biological tissue. Elastic wave propagation in the cornea is dispersive, similar to light refraction in different media, which depends on the frequency. The dispersion of the elastic wave within the

cornea can be quantified by calculating the phase velocity of various elastic wave frequencies (31). Thus, we quantified the corneal Young's modulus using the Lamb wave model based on the frequency-dependent phase velocity.

First, the Doppler phase shift $\Delta\varphi$ at each depth was extracted from the M-scan OCT images. The Lamb wave vibration displacement Δd was then calculated based on the Doppler phase shift $\Delta\varphi$ of the OCT signal according to the following equation (32,33):

$$\Delta d = \frac{\lambda_0}{4\pi n}\Delta\varphi \quad [1]$$

where λ_0 is the central wavelength of the swept laser source, and n is the refractive index of the sample.

A two-dimensional (2D) fast Fourier transform (FFT) was then applied to map the spatiotemporal displacement image of the Lamb waves to the wavenumber frequency domain (34,35). For each frequency, the wavenumber k was selected by identifying the point with the maximum intensity at that frequency. Subsequently, the phase velocity c_L at the frequency was calculated with Eq. [2] (36,37):

$$c_L = \frac{2\pi f}{k} \quad [2]$$

where f is the frequency, and k is the wavenumber.

Finally, the Young's modulus of the cornea was determined according to the following formula:

$$E = \frac{9\rho \times c_L^4}{\left(\pi \times f \times h\right)^2} \quad [3]$$

where ρ is the density of the cornea (1,062 kg/m^3) (38), and h is the corneal thickness.

Animals and study design

Experiments were performed under a project license (No. zocnc2023-0033) granted by the Animal Ethics Committee of Nanchang Eye Hospital, Zhongshan Eye Center, Sun Yat-sen University, and in compliance with institutional guidelines for the care and use of animals. Eighteen healthy adult male New Zealand rabbits (3 to 3.5 kg, aged 4 to 5 months) were obtained from the Animal Center of Nanchang University. Fifteen of these rabbits were randomly assigned to five experimental groups (n=3 per group) and administered a different UVA energy dose (5.4, 15, 25, 35, or 45 J/cm^2). The energy doses of 5.4 and 15 J/cm^2 have previously been used in clinic (4,7). One study indicated there to be no threshold detected up to 20 J/cm^2 for cross-linking in enhancing corneal biomechanics (39). Furthermore, recent research has demonstrated the efficacy of a 30 J/cm² energy dose in enhancing corneal biomechanics (30,40). Thus, to maximally induce changes in corneal biomechanics, the highest energy dose was set to 45 J/cm^2. The remaining three rabbits were set as the control group: they received only riboflavin instillation and were not exposed to UVA irradiation (0 J/cm^2).

The PiXL procedure was randomly administered to either the left or right eye of each rabbit. Two OCE measurements were performed on the treated eye of each rabbit. The first OCE measurement was obtained 3 days prior to PiXL. The second OCE measurement was performed 1 week after PiXL treatment, as normal corneal transparency and thickness could be restored in rabbit corneas following cross-linking within this time frame (41). All OCE measurements and PiXL treatments were performed under general anesthesia via an intramuscular injection of xylazine (5 mg/kg) and ketamine (35 mg/kg). During the measurements, the cornea was coupled with the ultrasmall transducer probe via a medical ultrasonic coupling agent, as shown in *Figure 2A*. Intraocular pressure (IOP) was measured with a rebound tonometer (iCare PRO, iCare, Vantaa, Finland) during each OCE measurement. The IOP in the rabbit eye, under general anesthesia and in the prone position, ranged between 13 and 15 mmHg. In our study, we assessed the changes in corneal Young's modulus (E) induced by PiXL treatment. The change in Young's modulus (ΔE) was calculated as follows: ΔE = Epost – Epre, where Epost is the postoperative value, and Epre is the preoperative value. The relative change was considered to be the percentage change in Young's modulus (ΔE%), which was calculated as follows: ΔE% = ΔE/Epre.

Pre- and post-PiXL examinations

Corneal tomography was measured with a Pentacam imaging system (Pentacam HR, Oculus, Wetzlar, Germany) under general anesthesia 3 days before PiXL and 1 week after PiXL. Anesthetized rabbits were placed on a customized lifting table, and their head and eye positions were consistently maintained by an assistant. All Pentacam measurements were performed by the same trained operator (HY). The Pentacam HR measurements were used to derive central corneal mean keratometry (K_m) readings, calculated as the average of the flat K reading and steep K reading. PiXL-induced changes in corneal K_m were calculated as follows: $\Delta K_m = \left(K_m pre - K_m post\right)$, where $K_m pre$ is the

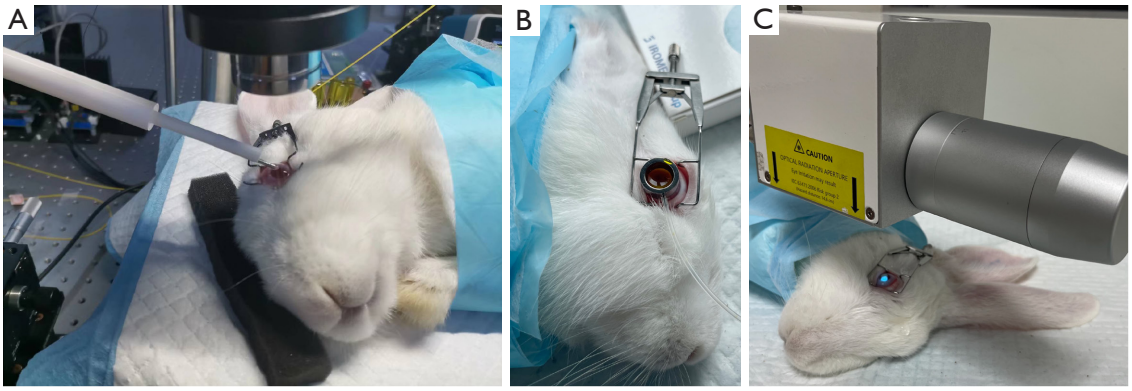

Figure 2 Experimental procedures conducted *in vivo* on rabbit corneas. (A) Photograph of the ultrasmall ultrasound transducer with the experimental rabbit in the optical coherence elastography experiment. (B) A retention ring was applied, and riboflavin was filled within the ring. (C) A 4-mm diameter yellow bright spot appeared on the cornea due to a photochemical reaction during cross-linking.

preoperative K_m, and $K_m post$ is the postoperative K_m.

PiXL protocol

All PiXL procedures were performed under general anesthesia. The anesthesia was administered as described above. A lid speculum was applied to hold the eyelids of each rabbit, and a retention ring at negative pressure was placed exactly central to the cornea. The corneal epithelium was not removed. Transepithelial riboflavin (Ribocross, Iromed Group, Rome, Italy) (42) drops were placed into the ring until the corneal surface was submerged (see *Figure 2B*). After 15 minutes, the ring was removed, and the corneal surface was rinsed with lactated Ringer's solution. The above-described process constituted one soak cycle. Subsequently, the central zone of the cornea was irradiated with a 4-mm diameter spot of 365 nm of UVA at 30 mW/cm^2 with the CF-X linker (IROMED Group) (42) in pulsed mode (1 second on, 1 second off). Due to the photochemical reaction of riboflavin, a 4-mm diameter yellow bright spot appeared on the cornea (see *Figure 2C*). As inadequate intrastromal riboflavin concentration could influence reaction effects (43,44), different soak cycles and irradiation times were employed for each energy dose, as described in previous studies (30,40). A detailed description of the group treatments is provided below:

For the control group (0 J/cm^2), after one soaking cycle, the rabbit was placed in a dark room for 2 hours to prevent exposure to UVA radiation from daylight. For group I (5.4 J/cm^2), after one soak cycle, the cornea was irradiated for 6 minutes. For group II (15 J/cm^2), after one soak cycle, the cornea was irradiated for 17 minutes. For group III (25 J/cm^2), after the first soak cycle, the cornea was irradiated for 17 minutes, a second soak cycle was performed, and then the cornea was irradiated again for 11 minutes.

For group IV (35 J/cm^2), after the first soak cycle, the cornea was irradiated for 17 minutes, a second soak cycle was performed, and the cornea was then irradiated again for 11 minutes. Finally, a third soak cycle was performed, which was followed by irradiation of the cornea for 11 minutes. For group V (45 J/cm^2), the same protocol as in group IV was performed, but an additional soak cycle was performed and followed by irradiation of the cornea for 11 minutes.

After PiXL, all rabbits received 0.5% levofloxacin drops four times a day for 7 days to prevent infection.

Statistical analysis

Paired *t*-tests were used to compare the pre- and post-PiXL values. One-way analysis of variance (ANOVA) and least significant difference (LSD) post hoc tests were used to determine the statistically significant differences between the means of the five groups. The association between ΔK_m and ΔE% was assessed by calculating the Pearson correlation coefficient (r). A P value less than 0.05 was considered statistically significant.

Results

Corneal topography and keratometry

The K_m values before and after PiXL are shown in *Table 1*.

Table 1 Changes in keratometry after PiXL treatments with different UVA doses

Group	Ultraviolet-A dose (J/cm^2)	K_m (D)		P value
		Before PiXL	After PiXL	
I	5.4	47.47±0.74	47.07±0.81	0.02
II	15	48.10±1.11	47.23±1.15	0.01
III	25	49.73±0.55	48.43±0.65	0.002
IV	35	50.33±1.06	48.23±1.15	0.003
V	45	48.70±0.79	48.27±0.78	0.006
Control	0	46.37±0.21	46.00±0.26	0.008

Values are mean ± standard deviation. PiXL, photorefractive intrastromal corneal cross-linking; UVA, ultraviolet-A; K_m, central corneal mean keratometry; D, diopter.

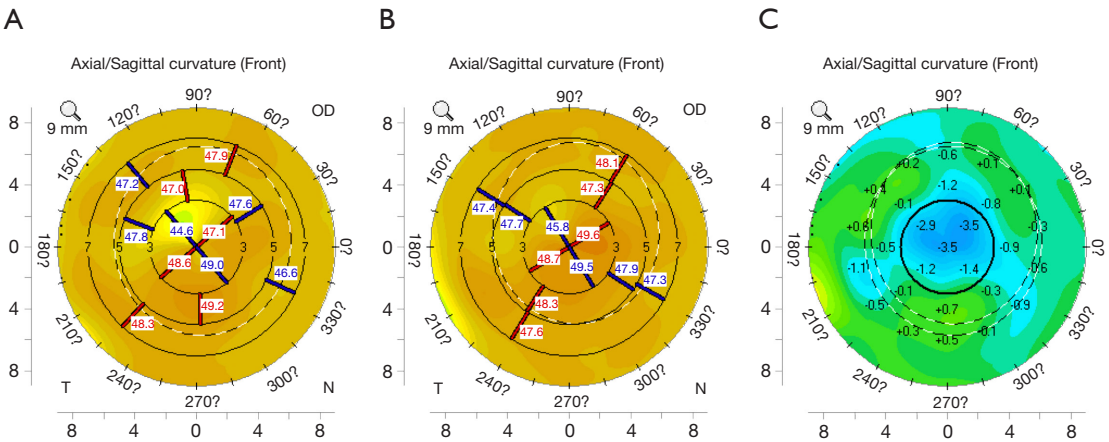

Figure 3 Scheimpflug-derived difference map of the axial curvature in group III (25 J/cm^2). (A) One week after PiXL. (B) Three days before PiXL. (C) The difference map. OD, oculus dexter; PiXL, photorefractive intrastromal corneal cross-linking.

A significant reduction in K_m after PiXL was observed in all experimental groups (all P values <0.05). *Figure 3* presents example tomography data before and after PiXL with a 25 J/cm^2 UVA dose. The differences in ΔK_m between the five experimental groups are presented in *Table 2*. Statistically significant ΔK_m between-group differences were observed between group I (5.4 J/cm^2) through to group IV (35 J/cm^2). *Figure 4* graphically illustrates the effects of different UVA doses on corneal curvature and biomechanical properties. The mean value of ΔK_m increased with increasing UVA dose from group I to group IV (35 J/cm^2), ranging from 0.40 to 2.10 diopters (D), as depicted in *Figure 4A*. Interestingly, group V (45 J/cm^2), despite receiving the highest UVA dose, did not exhibit the most significant change in ΔK_m.

Quantification of the corneal Young's modulus

To facilitate understanding, we describe one of the rabbit corneas prior to PiXL treatment to illustrate the process for evaluating the corneal biomechanics. *Figure 5* is a graphical representation of the imaging results of the normal cornea. *Figure 5A* shows a 2D OCT image of the rabbit cornea. When ARF excitation was applied, an elastic wave propagated from the ultrasound focus to the surrounding tissue. The 2D time-lapse Doppler OCT images shown in *Figure 5B-5E* are a visualization of the Lamb wave propagation. In the images, the different colors represent distinct vibration directions and displacements. In *Figure 5B*, the white and red arrows indicate the ARF excitation position and propagation direction, respectively.

Table 2 Comparison of ΔK_m, ΔE, and ΔE% among the groups

Group	Ultraviolet-A dose (J/cm^2)	ΔK_m(D)	ΔE (kPa)	ΔE%
I	5.4	0.40±0.10^{d}	9.17±2.85^{d}	0.26±0.03^{e}
II	15	0.87±0.15^{c}	19.87±5.66^{cd}	0.55±0.05^{d}
III	25	1.30±0.10^{b}	37.3±9.85^{bc}	1.07±0.06^{c}
IV	35	2.10±0.20^{a}	48.03±12.66^{ab}	1.28±0.08^{b}
V	45	0.43±0.06^{d}	62.53±16.25^{a}	1.71±0.09^{a}
Control	0	0.37±0.06^{d}	3.52±1.75^{d}	0.09±0.05^{f}
F ratio	–	94.104	17.051	300.969
P value	–	<0.001	<0.001	<0.001

Values are mean ± standard deviation. Comparisons between five groups were conducted via one-way analysis of variance followed by the least significant difference post hoc test. Different letters (^{a}, ^{b}, ^{c}, ^{d}, etc.) in the same column indicate a statistically significant difference to other groups (P<0.05). ΔK_m, change in the mean keratometry; ΔE, change in Young's modulus; ΔE%, percentage change in Young's modulus; D, diopter.

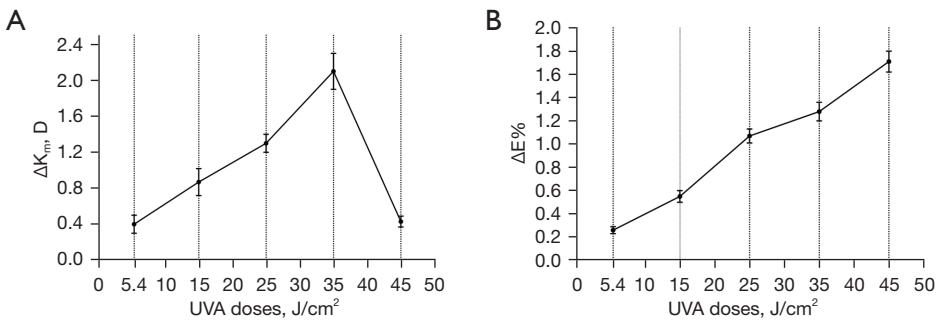

Figure 4 The effects of UVA doses on corneal curvature and biomechanics. (A) Change in ΔK_m with increasing UVA energy dose. (B) Change in ΔE% with increasing UVA energy dose. ΔK_m, change in the mean keratometry; UVA, ultraviolet-A; ΔE%, percentage change in Young's modulus.

Figure 5F shows a spatiotemporal displacement image of the cornea obtained by reslicing the Doppler OCT images along the depth direction at the depth indicated by the yellow line in *Figure 5A*. Subsequently, the wavenumber-frequency domain map (*Figure 6A*) was obtained using the FFT, as described in the Methods section. Next, Eq. [2] was used to obtain the dispersion curve via the identification of the maximum wavenumber value at each frequency (*Figure 6B*). Finally, fitting to the dispersion curve indicated that the phase velocity value at the selected depth was approximately 3.48 m/s, and Young's modulus of 38.6 kPa was calculated according to Eq. [3].

The Young's modulus at all available depths in the cornea was obtained by repeating the quantification process described above. Specifically, we acquired phase velocity at 10 depth locations, from the anterior to the posterior stroma in 30 μm steps, to determine the corresponding Young's modulus. Subsequently, a depth-resolved image of the Young's modulus was obtained by directly mapping the Young's modulus to the corresponding structure, as shown in *Figure 7A*. The corneal Young's modulus exhibited a gradual decrease from the anterior stroma to the posterior stroma. *Figure 7B*-*7F* illustrates the depth-resolved corneal biomechanical results for each group after PiXL. In all five groups, a notable enhancement in Young's moduli was observed, which was accompanied by a depth-dependent decrease in moduli values. Furthermore, as evident from *Figure 7B*-*7F*, the Young's modulus of the cornea incrementally increased as the UVA energy dose increased.

To quantitatively assess changes in corneal biomechanics,

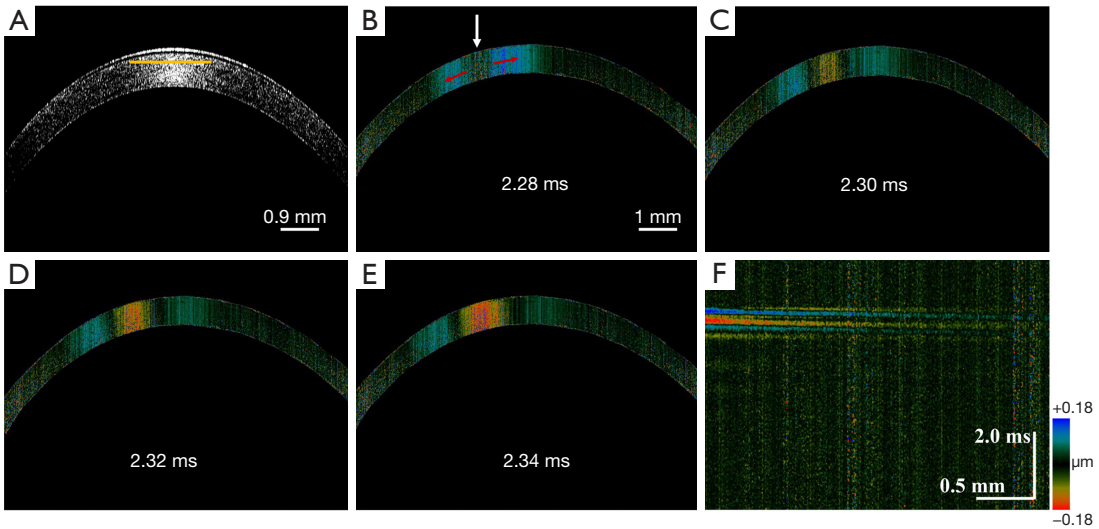

Figure 5 Imaging results of the normal cornea. (A) The two-dimensional OCT image of the *in vivo* healthy cornea, with the yellow line indicating the depth direction at which the Doppler OCT images were resliced to obtain the spatiotemporal displacement image shown in (F). (B-E) The time-lapse Doppler OCT B-scans of the healthy rabbit cornea, with the white and red arrows indicating the excitation position and the direction of wave propagation, respectively. (F) The spatiotemporal displacement image of the Lamb wave. OCT, optical coherence tomography.

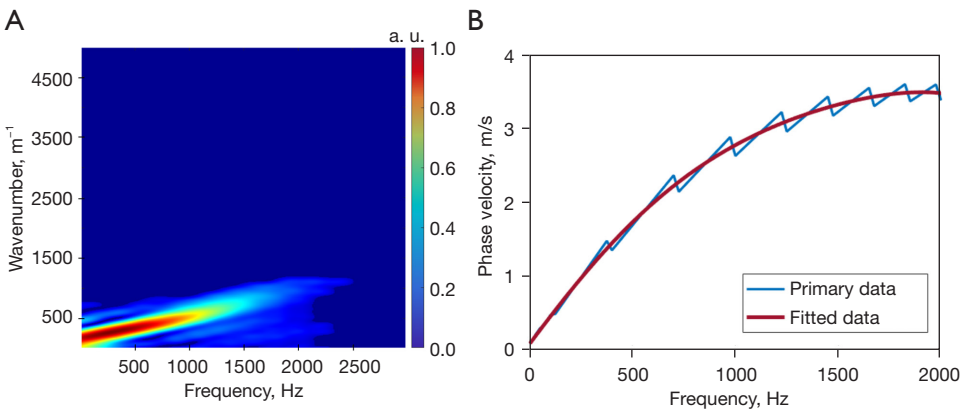

Figure 6 Phase velocity of the Lamb wave calculation. (A) Wavenumber frequency domain map. (B) Phase velocity dispersion curve with frequency.

we conducted a comparative analysis of the average Young's modulus values of the cornea before and after PiXL. *Table 3* shows the average Young's modulus before and after PiXL for each group. A significant increase in Young's moduli after PiXL was observed in all experimental groups (all P values <0.05). There was no significant difference in the control group. The differences in ΔE and ΔE% for the five experimental groups are shown in *Table 2*. There were statistically significant between-group differences in ΔE% between the five groups. As the UVA dose increased from group I (5.4 J/cm^2) to group V (45 J/cm^2), the mean value of ΔE% also increased, as shown in *Figure 4B*. The values ranged from 0.26 to 1.71.

Corneal biomechanics and keratometry

A statistically significant positive correlation was found between ΔE% and ΔK_m in groups I to IV (r=0.983; P<0.001;

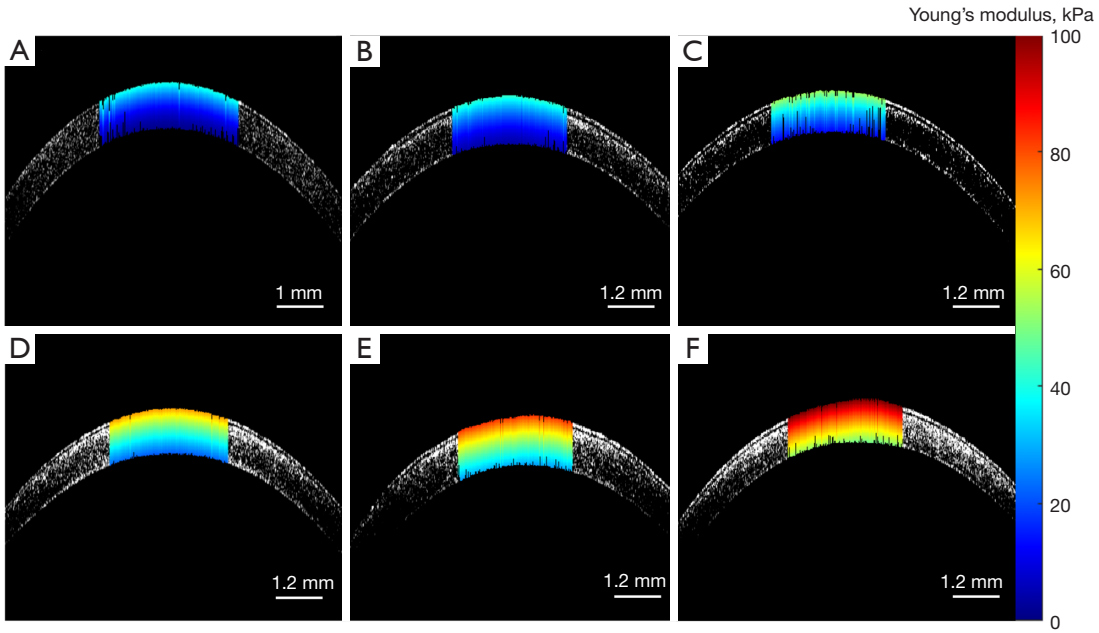

Figure 7 Depth-resolved distribution of the corneal Young's modulus. (A) A normal cornea. (B-F) Cornea after PiXL treatment with ultraviolet-A doses of 5.4, 15, 25, 35, and 45 J/cm^2, respectively. Different colors correspond to different values of the Young's modulus, as indicated by the color bar. PiXL, photorefractive intrastromal corneal crosslinking.

Table 3 Changes in corneal Young's modulus after PiXL with different ultraviolet-A doses

Group	Ultraviolet-A dose (J/cm^2)	Young's modulus (kPa)		P value
		Before PiXL	After PiXL	
I	5.4	34.67±6.95	43.83±9.80	0.031
II	15	35.53±7.35	55.40±13.00	0.026
III	25	34.57±7.25	71.87±17.10	0.022
IV	35	37.23±7.55	85.27±20.20	0.022
V	45	36.30±7.60	95.50±19.02	0.012
Control	0	37.90±4.61	40.23±6.37	0.672

Values are mean ± standard deviation. PiXL, photorefractive intrastromal corneal crosslinking.

Figure 8).

Discussion

PiXL aims to modify the biomechanical properties of the cornea, altering its curvature and refractive power to correct refractive errors (6,10,11). The ultimate goal is to enhance the precision and range of customized PiXL treatments for myopia correction by leveraging the dose-effect relationship between corneal biomechanics and curvature. To accomplish this, an appropriate method for quantifying corneal biomechanics *in vivo* is essential. Previous *in vivo* attempts to measure corneal biomechanical properties have included corneal hysteresis and corneal resistance factor derived from the ocular response analyzer and the stiffness Parameter obtained from corneal visualization Scheimpflug technology (45,46). Although these parameters have been used to diagnose keratoconus and assess CXL, their utility remains under debate (13). Additionally, while studies have observed a decrease in corneal curvature in keratoconic

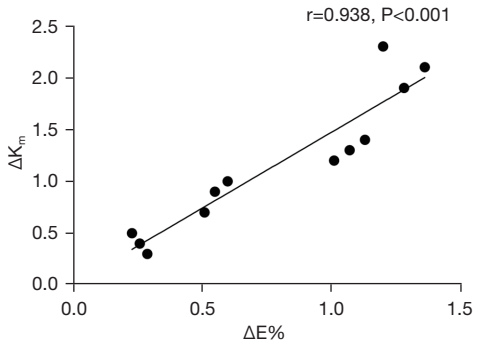

Figure 8 Scatter plot showing the correlation between ΔE% and ΔK_m. ΔK_m, change in the mean keratometry; ΔE%, percentage change in Young's modulus.

eyes following CXL, no research has used the changes in these parameters to investigate the relationship between biomechanical alterations and curvature reduction. Recent studies have reported there to be a correlation between the stress-strain index derived from corneal visualization Scheimpflug technology and corneal curvature radius in myopic populations (47,48). Nevertheless, these studies were predominantly qualitative in nature and did not quantify the specific relationship between biomechanical changes and alterations in corneal curvature. Studies using stress-strain extensometry have demonstrated that increasing doses of UVA energy in the range of 0–5.4 J/cm^2 significantly enhance corneal strength (49). However, these *in vitro* experiments are unable to monitor biomechanical changes *in vivo*, limiting the ability to establish further correlations with *in vivo* curvature alterations.

The OCE technique has been used for the quantitative assessment of corneal biomechanics and is viewed as the most promising ocular elastography technique for clinical application (23). A recent study using OCE on *ex vivo* porcine eyes demonstrated that refractive changes are directly related to corneal biomechanics as calculated by axial strain changes (50). To the best of our knowledge, no *in vivo* studies have quantitatively compared the changes in corneal biomechanics to the alterations in corneal curvature after PiXL via the Young's modulus values derived from the ARF-OCE system. In this study, we employed an ARF-OCE technique for the *in vivo* quantitative assessment of corneal biomechanical changes following PiXL treatment. Moreover, the Lamb wave dispersion induced by the anisotropic biological properties of the cornea was obtained, and the dispersion curves of the Lamb wave phase velocity across various frequencies was derived using the FFT method.

Experiments were first performed on healthy *in vivo* rabbit corneas, in which the 2D OCT maps and Lamb wave propagations were imaged. Subsequently, the FFT of the spatiotemporal displacement image of the Lamb waves at the selected depth location was applied to generate the wavenumber-frequency domain map. Finally, the Lamb wave velocity, based on the frequency-dependent phase velocity curve, was determined to be 3.48 m/s, which is consistent with results from previous studies (29,30). The corneal Young's modulus was subsequently calculated to be 38.6 kPa, and accordingly, the Young's modulus at all available depth locations was obtained to map the depth-resolved image, using the same calculation steps. As shown in *Figure 7A*, the corneal Young's modulus gradually decreased from anterior to the posterior stroma, which is in line with previous research (30,31,51). Additionally, OCE measurements were performed on all rabbit corneas before and after PiXL (n=18), and the Young's modulus of each cornea was determined. The depth-resolved 2D biomechanical distribution map after PiXL was then obtained using the same method. As illustrated in *Figure 7B-7F*, there was a preferential stiffening of the anterior stroma in each group. This can be attributed to the fact that the crosslinking effect is strongest in the anterior stroma (11,52,53). More importantly, the results indicate that the corneal Young's modulus increases with increasing UVA energy dose. Furthermore, *Table 3* summarizes the changes in average corneal Young's modulus with five UVA energy doses. These results demonstrate that the increase in UVA energy doses enhances corneal biomechanics, and our system is capable of quantifying the differences in Young's modulus due to different UVA energy doses.

In our quantitative investigation of the dose-effect relationship in PiXL, we focused on correlating Young's modulus values with corneal curvature. As indicated in *Table 2*, statistically significant between-group differences in both ΔE% and ΔK_m were observed among groups I to IV. These values increased with the UVA energy dose, as shown in *Figure 4*. Importantly, a comparison of the data across groups I to IV revealed a positive correlation between ΔE% and ΔK_m (*Figure 8*). This observed correlation suggests that ΔE% may be a promising quantitative biomechanical parameter for determining the dose-effect relationship in PiXL treatments. Therefore, the ARF-OCE system could be used to noninvasively measure ΔE% *in vivo*, thereby facilitating the quantitative determination of the dose-effect relationship in PiXL.

Furthermore, the results indicated that ΔE% values of the corneas in group V (45 J/cm^2) were higher than those in group IV (35 J/cm^2). However, it is worth noting that the observed reduction in K_m was markedly lower in group V than group IV. We hypothesize that this phenomenon may be attributed to the 45 J/cm^2 energy dose inducing excessive stiffness in the tissues surrounding the irradiated area. This is supported by a previous study, which demonstrated that the stiffening effect of localized corneal cross-linking extends beyond the irradiated area (54). In normal corneas, the areas where collagen fibers are densely interwoven exhibit greater stiffness and enhanced resistance to the outward forces generated by IOP as compared to less densely interwoven regions. These variations in resistance across the corneal surface may account for the observed deviations in corneal topography in normal corneas (10). In PiXL, irradiation of the central cornea modifies the tensile strength of its collagen, which potentially enhances the resistance of the central cornea against deformation under IOP, thereby decreasing the central corneal curvature. However, excessively high UVA energy may cause excessive stiffening in surrounding areas. This disproportionate stiffening may attenuate the flattening effect of the central corneal region. Therefore, future studies should investigate UVA energies between 35 and 45 J/cm^2 to determine the inflection point of the ΔE% value between 1.28 and 1.71 at which K_m stops decreasing and begins to increase.

We further observed a statistically significant change in corneal curvature in the control group (*Table 1*), and this change in curvature within the control group was comparable to that observed in group I (*Table 2*). Hence, the curvature changes observed in group I may not be solely attributable to the surgical intervention. In contrast, the changes in groups II, III, and IV were significantly different and more pronounced compared to those of the control group. The slight curvature change in the control group may be attributed to measurement errors or natural growth variations. Despite the lack of a significant difference in curvature between group I and the control group, group I demonstrated a significant enhancement in ΔE% (*Table 2*). Therefore, despite our finding that the 5.4 J/cm² energy dose enhances corneal biomechanics and previous studies proving its efficacy in treating keratoconus, it is insufficient to induce meaningful alterations in corneal curvature in normal corneas. This observation might explain why an energy dose of at least 10 J/cm^2 has been consistently used in clinical applications of PiXL (1-3) and suggests that ΔE% may need to exceed a certain threshold to significantly impact changes in corneal keratometry.

There are some limitations to be noted regarding our study. First, although no significant complications were observed in rabbit corneas treated with PiXL, the potential risk of increased UVA flux to human corneal endothelial cells must be carefully considered in practical applications. Second, the impact of IOP on corneal biomechanics was not analyzed; however, the IOP fluctuations in live rabbit eyes during the experiments were measured to be within 2 mmHg. A previous study reported that fluctuations within this range have a minor impact on corneal wave speed, implying a correspondingly small effect on the corneal Young's modulus as measured by wave speed (55). Therefore, it can be surmised that the statistical results were not significantly affected. Finally, this study did not account for the influence of changes in corneal thickness on curvature alterations, which should be considered in future research in providing a more comprehensive analysis.

In this study, we aimed to use the proposed ARF-OCE system to generate depth-resolved maps of corneal Young's modulus before and after PiXL. Importantly, to study the dose-effect relationship, we correlated corneal curvature data with a quantitative biomechanical parameter. However, the biomechanical alterations induced by PiXL are complex. Accurate determination of the dose-effect relationship requires testing large numbers of corneas and understanding the long-term relationship between changes in corneal biomechanics and curvature. Our study represents an important step toward achieving these objectives. Moreover, although our study realized 2D biomechanical mapping, a comprehensive understanding of the relationship between corneal biomechanics and curvature necessitates the advancement into 3D elastography. To enable rapid 3D elastography, several challenges must be addressed. Initially, the scanning speed must be enhanced to reduce the data acquisition time. High-speed lasers are effective tools for increasing the acquisition speed. Additionally, the scanning range of the SS-OCT system must be expanded to cover a larger area of corneal tissue. This expansion can be achieved by incorporating an electric moving stage into the sample arm. Finally, the development of 3D elastography algorithms is imperative.

Conclusions

We developed an ARF-OCE system equipped with an ultrasmall ultrasound transducer for the *in vivo* assessment of biomechanical properties in the rabbit cornea. We

demonstrated the capability of the proposed ARF-OCE system to quantitatively assess changes in corneal biomechanics following PiXL with five different UVA doses: 5.4, 15, 25, 35, and 45 J/cm^2. The results showed that with increasing UVA energy dose, the corneal Young's modulus incrementally increases. More importantly, our findings suggest that ΔE% could serve as a valuable novel quantitative biomechanical parameter for determining the dose-effect relationship in PiXL treatment. This work offers a preliminary technique that may facilitate the quantitative determination of the dose-effect relationship in PiXL and, with further optimization, may have clinical applications.

Acknowledgments

Funding: This work was supported by the National Natural Science Foundation of China (No. 82360215), the Natural Science Foundation of Jiangxi Province (No. 20212BAG70033), and the Natural Science Foundation of Jiangxi Province (No. 20202BBG72004).

Footnote

Conflicts of Interest: All authors have completed the ICMJE uniform disclosure form (available at https://qims.amegroups.com/article/view/10.21037/qims-24-590/coif). The authors have no conflicts of interest to declare.

Ethical Statement: The authors are accountable for all aspects of the work in ensuring that questions related to the accuracy or integrity of any part of the work are appropriately investigated and resolved. Experiments were performed under a project license (No. zocnc2023-0033) granted by the Animal Ethics Committee of Nanchang Eye Hospital, Zhongshan Eye Center, Sun Yat-sen University, and in compliance with institutional guidelines for the care and use of animals.

References

1. Lim WK, Soh ZD, Choi HKY, Theng JTS. Epithelium-on photorefractive intrastromal cross-linking (PiXL) for reduction of low myopia. Clin Ophthalmol 2017;11:1205-11.
2. Elling M, Kersten-Gomez I, Dick HB. Photorefractive intrastromal corneal crosslinking for the treatment of myopic refractive errors: Six-month interim findings. J Cataract Refract Surg 2017;43:789-95.
3. Elling M, Kersten-Gomez I, Dick HB. Photorefractive intrastromal corneal crosslinking for treatment of myopic refractive error: Findings from 12-month prospective study using an epithelium-off protocol. J Cataract Refract Surg 2018;44:487-95.
4. Sachdev GS, Ramamurthy S, Dandapani R. Photorefractive intrastromal corneal crosslinking for treatment of low myopia: clinical outcomes using the transepithelial approach with supplemental oxygen. J Cataract Refract Surg 2020;46:428-33.
5. Kohlhaas M. Iatrogenic Keratectasia: A Review. Klin Monbl Augenheilkd 2015;232:765-72.
6. Wollensak G, Spoerl E, Seiler T. Stress-strain measurements of human and porcine corneas after riboflavin-ultraviolet-A-induced cross-linking. J Cataract Refract Surg 2003;29:1780-5.
7. Subasinghe SK, Ogbuehi KC, Dias GJ. Current perspectives on corneal collagen crosslinking (CXL). Graefes Arch Clin Exp Ophthalmol 2018;256:1363-84.
8. Singh M, Li J, Han Z, Vantipalli S, Liu CH, Wu C, Raghunathan R, Aglyamov SR, Twa MD, Larin KV. Evaluating the Effects of Riboflavin/UV-A and Rose-Bengal/Green Light Cross-Linking of the Rabbit Cornea by Noncontact Optical Coherence Elastography. Invest Ophthalmol Vis Sci 2016;57:OCT112-20.
9. Ferguson TJ, Singuri S, Jalaj S, Ford MR, De Stefano VS, Seven I, Dupps WJ Jr. Depth-resolved Corneal Biomechanical Changes Measured Via Optical Coherence Elastography Following Corneal Crosslinking. Transl Vis Sci Technol 2021;10:7.
10. Winkler M, Chai D, Kriling S, Nien CJ, Brown DJ, Jester B, Juhasz T, Jester JV. Nonlinear optical macroscopic assessment of 3-D corneal collagen organization and axial biomechanics. Invest Ophthalmol Vis Sci 2011;52:8818-27.
11. Wollensak G, Wilsch M, Spoerl E, Seiler T. Collagen fiber diameter in the rabbit cornea after collagen crosslinking by riboflavin/UVA. Cornea 2004;23:503-7.
12. Jędzierowska M, Koprowski R. Novel dynamic corneal response parameters in a practice use: a critical review.

Biomed Eng Online 2019;18:17.
13. Bak-Nielsen S, Pedersen IB, Ivarsen A, Hjortdal J. Dynamic Scheimpflug-based assessment of keratoconus and the effects of corneal cross-linking. J Refract Surg 2014;30:408-14.
14. Gkika M, Labiris G, Giarmoukakis A, Koutsogianni A, Kozobolis V. Evaluation of corneal hysteresis and corneal resistance factor after corneal cross-linking for keratoconus. Graefes Arch Clin Exp Ophthalmol 2012;250:565-73.
15. Greenstein SA, Fry KL, Hersh PS. In vivo biomechanical changes after corneal collagen cross-linking for keratoconus and corneal ectasia: 1-year analysis of a randomized, controlled, clinical trial. Cornea 2012;31:21-5.
16. Goldich Y, Barkana Y, Morad Y, Hartstein M, Avni I, Zadok D. Can we measure corneal biomechanical changes after collagen cross-linking in eyes with keratoconus?--a pilot study. Cornea 2009;28:498-502.
17. Kling S, Hafezi F. Corneal biomechanics - a review. Ophthalmic Physiol Opt 2017;37:240-52.
18. Murphy MC, Huston J 3rd, Ehman RL. MR elastography of the brain and its application in neurological diseases. Neuroimage 2019;187:176-83.
19. Qian X, Li R, Lu G, Jiang L, Kang H, Kirk Shung K, Humayun MS, Zhou Q. Ultrasonic elastography to assess biomechanical properties of the optic nerve head and peripapillary sclera of the eye. Ultrasonics 2021;110:106263.
20. Li Y, Zhu J, Chen JJ, Yu J, Jin Z, Miao Y, Browne AW, Zhou Q, Chen Z. Simultaneously imaging and quantifying in vivo mechanical properties of crystalline lens and cornea using optical coherence elastography with acoustic radiation force excitation. APL Photonics 2019;4:106104.
21. Zhu Y, Zhang Y, Shi G, Xue Q, Han X, Ai S, Shi J, Xie C, He X. Quantification of iris elasticity using acoustic radiation force optical coherence elastography. Appl Opt 2020;59:10739-45.
22. Du Z, Li R, Qian X, Lu G, Li Y, He Y, Qu Y, Jiang L, Chen Z, Humayun MS, Chen Z, Zhou Q. Quantitative confocal optical coherence elastography for evaluating biomechanics of optic nerve head using Lamb wave model. Neurophotonics 2019;6:041112.
23. Kirby MA, Pelivanov I, Song S, Ambrozinski Ł, Yoon SJ, Gao L, Li D, Shen TT, Wang RK, O'Donnell M. Optical coherence elastography in ophthalmology. J Biomed Opt 2017;22:1-28.
24. Li R, Du Z, Qian X, Li Y, Martinez-Camarillo JC, Jiang L, Humayun MS, Chen Z, Zhou Q. High resolution optical coherence elastography of retina under prosthetic electrode. Quant Imaging Med Surg 2021;11:918-27.
25. Qian X, Li R, Li Y, Lu G, He Y, Humayun MS, Chen Z, Zhou Q. In vivo evaluation of posterior eye elasticity using shaker-based optical coherence elastography. Exp Biol Med (Maywood) 2020;245:282-8.
26. Jin Z, Zhou Y, Shen M, Wang Y, Lu F, Zhu D. Assessment of corneal viscoelasticity using elastic wave optical coherence elastography. J Biophotonics 2020;13:e201960074.
27. Vellara HR, Patel DV. Biomechanical properties of the keratoconic cornea: a review. Clin Exp Optom 2015;98:31-8.
28. Roberts CJ, Dupps WJ Jr. Biomechanics of corneal ectasia and biomechanical treatments. J Cataract Refract Surg 2014;40:991-8.
29. Zhao Y, Yang H, Li Y, Wang Y, Han X, Zhu Y, Zhang Y, Huang G. Quantitative Assessment of Biomechanical Properties of the Human Keratoconus Cornea Using Acoustic Radiation Force Optical Coherence Elastography. Transl Vis Sci Technol 2022;11:4.
30. Zhu Y, Zhao Y, Shi J, Gomez Alvarez-Arenas TE, Yang H, Cai H, Zhang D, He X, Wu X. Novel acoustic radiation force optical coherence elastography based on ultrasmall ultrasound transducer for biomechanics evaluation of in vivo cornea. J Biophotonics 2023;16:e202300074.
31. Wang S, Larin KV. Noncontact depth-resolved micro-scale optical coherence elastography of the cornea. Biomed Opt Express 2014;5:3807-21.
32. Qi W, Chen R, Chou L, Liu G, Zhang J, Zhou Q, Chen Z. Phase-resolved acoustic radiation force optical coherence elastography. J Biomed Opt 2012;17:110505.
33. Zhao Y, Chen Z, Saxer C, Xiang S, de Boer JF, Nelson JS. Phase-resolved optical coherence tomography and optical Doppler tomography for imaging blood flow in human skin with fast scanning speed and high velocity sensitivity. Opt Lett 2000;25:114-6.
34. Kemao Q. Two-dimensional windowed Fourier transform for fringe pattern analysis: Principles, applications and implementations. Opt Lasers Eng 2007;45:304-17.
35. Kijanka P, Urban MW. Local Phase Velocity Based Imaging of Viscoelastic Phantoms and Tissues. IEEE Trans Ultrason Ferroelectr Freq Control 2021;68:389-405.
36. Zhou K, Li C, Chen S, Nabi G, Huang Z. Feasibility study of using the dispersion of surface acoustic wave impulse for viscoelasticity characterization in tissue mimicking phantoms. J Biophotonics 2019;12:e201800177.

37. Zhou K, Le N, Huang Z, Li C. High-intensity-focused ultrasound and phase-sensitive optical coherence tomography for high resolution surface acoustic wave elastography. J Biophotonics 2018. doi: 10.1002/jbio.201700051.
38. Kampmeier J, Radt B, Birngruber R, Brinkmann R. Thermal and biomechanical parameters of porcine cornea. Cornea 2000;19:355-63.
39. Fischinger I, Reifeltshammer SA, Seiler TG, Nambiar MH, Komninou MA, Büchler P, Wendelstein J, Langenbucher A, Bolz M. Analysis of Biomechanical Response After Corneal Crosslinking with Different Fluence Levels in Porcine Corneas. Curr Eye Res 2023;48:719-23.
40. Zhao Y, Zhu Y, Yan Y, Yang H, Liu J, Lu Y, Li Y, Huang G. In Vivo Evaluation of Corneal Biomechanics Following Cross-Linking Surgeries Using Optical Coherence Elastography in a Rabbit Model of Keratoconus. Transl Vis Sci Technol 2024;13:15.
41. Hovakimyan M, Guthoff R, Knappe S, Zhivov A, Wree A, Krüger A, Heisterkamp A, Stachs O. Short-term corneal response to cross-linking in rabbit eyes assessed by in vivo confocal laser scanning microscopy and histology. Cornea 2011;30:196-203.
42. Caruso C, Costagliola C, Troisi S, Epstein RL. Compaction of very thin corneas from ultraviolet A riboflavin-vitamin E transepithelial cross-linking. Exp Eye Res 2021;205:108484.
43. Lombardo G, Villari V, Micali NL, Leone N, Labate C, De Santo MP, Lombardo M. Non-invasive optical method for real-time assessment of intracorneal riboflavin concentration and efficacy of corneal cross-linking. J Biophotonics 2018;11:e201800028.
44. Morgan SR, O'Brart DPS, Huang J, Meek KM, Hayes S. An in vitro investigation into the impact of corneal rinsing on riboflavin/UVA corneal cross-linking. Eye Vis (Lond) 2024;11:8.
45. Luce DA. Determining in vivo biomechanical properties of the cornea with an ocular response analyzer. J Cataract Refract Surg 2005;31:156-62.
46. Roberts CJ, Mahmoud AM, Bons JP, Hossain A, Elsheikh A, Vinciguerra R, Vinciguerra P, Ambrósio R Jr. Introduction of Two Novel Stiffness Parameters and Interpretation of Air Puff-Induced Biomechanical Deformation Parameters With a Dynamic Scheimpflug Analyzer. J Refract Surg 2017;33:266-73.
47. Chu Z, Ren Q, Chen M, Cheng L, Cheng H, Cui W, Bi W, Wu J. The relationship between axial length/corneal radius of curvature ratio and stress-strain index in myopic eyeballs: Using Corvis ST tonometry. Front Bioeng Biotechnol 2022;10:939129.
48. Chu Z, Ren Q, Su W, Cui W, Wu J. Effect of central corneal curvature on corneal material stiffness parameter acquired by dynamic corneal responses. Front Bioeng Biotechnol 2023;11:1237834.
49. Liu T, Shen M, Li H, Zhang Y, Mu B, Zhao X, Wang Y. Changes and quantitative characterization of hyper-viscoelastic biomechanical properties for young corneal stroma after standard corneal cross-linking treatment with different ultraviolet-A energies. Acta Biomater 2020;113:438-51.
50. Frigelli M, Büchler P, Kling S. Optomechanical assessment of photorefractive corneal cross-linking via optical coherence elastography. Front Bioeng Biotechnol 2023;11:1272097.
51. Thomasy SM, Raghunathan VK, Winkler M, Reilly CM, Sadeli AR, Russell P, Jester JV, Murphy CJ. Elastic modulus and collagen organization of the rabbit cornea: epithelium to endothelium. Acta Biomater 2014;10:785-91.
52. Kohlhaas M, Spoerl E, Schilde T, Unger G, Wittig C, Pillunat LE. Biomechanical evidence of the distribution of cross-links in corneas treated with riboflavin and ultraviolet A light. J Cataract Refract Surg 2006;32:279-83.
53. Wollensak G, Aurich H, Pham DT, Wirbelauer C. Hydration behavior of porcine cornea crosslinked with riboflavin and ultraviolet A. J Cataract Refract Surg 2007;33:516-21.
54. Webb JN, Langille E, Hafezi F, Randleman JB, Scarcelli G. Biomechanical Impact of Localized Corneal Cross-linking Beyond the Irradiated Treatment Area. J Refract Surg 2019;35:253-60.
55. Zvietcovich F, Nair A, Singh M, Aglyamov SR, Twa MD, Larin KV. In vivo assessment of corneal biomechanics under a localized cross-linking treatment using confocal air-coupled optical coherence elastography. Biomed Opt Express 2022;13:2644-54.

Cite this article as: Yang H, Shen Y, Chen Y, Yan Y, Li Y, Lu Y, Liu J, Yin X, Huang G, Zhao Y. Quantitative assessment of corneal biomechanical changes in vivo after photorefractive intrastromal corneal cross-linking using optical coherence elastography. Quant Imaging Med Surg 2024;14(10):7640-7653. doi: 10.21037/qims-24-590

